Singularity Analysis and Configuration Optimization of Two SGCMGs

Chengfei Yue, Cher Hiang Goh, Tong Heng Lee
Department of Electrical and Computer Engineering
National University of Singapore
Singapore, Singapore 117582
chengfei_yue@u.nus.edu, elegch@nus.edu.sg, eleleeth@nus.edu.sg

Qiang Shen
Temasek Laboratories
National University of Singapore
Singapore, Singapore 117411
tslshen@nus.edu.sg

Abstract— **In contrast to past studies that treat each configuration of Single Gimbal Control Moment Gyros (SGCMGs) individually, this paper introduces a unified coordinate frame such that two SGCMGs in arbitrary configuration can be transformed into a unified description. Using this description, the angle between two fixed gimbal axes becomes the unique parameter to determine the shape of the momentum envelope and various singular surface, which offers the convenience for singularity analysis and configuration optimization. For different angles of two gimbal axes, we investigate its corresponding singularity and provide a thorough analysis. Consequently, this angle is optimized from the viewpoint of maximizing the momentum envelope. This work may lay foundation for the application of two SGCMGs in satellite attitude control.**

TABLE OF CONTENTS

1. INTRODUCTION

For spacecraft, the whole angular momentum is conservative without the consideration of external disturbancies. Thus momentum exchange is an effective way in spacecraft attitude control. Actuators based on such a principle include Reaction Wheel (RW) and Control Moment Gyro (CMG). RW is a spinning rotor which can accelerate or decelerate during the control process. CMG is a device consisting of a rotor fixed on some gimbals. When the rotor velocity varies, it is the Variable Speed CMG (VSCMG).When the rotor rotates at a constant speed, CMGs can be divided into Single Gimbal CMG (SGCMG) and Double Gimbal CMG (DGCMG) categorized by the number of gimbals. Compared to the DGCMG and VSCMG, SGCMG has the advantage in mechanical simplicity from the hardware viewpoint. It also offers significant cost, power, weight, and reliability advantages over DGCMGs [1] and owns the significant torque amplification property; i.e. the produced output torque is much larger than the provided gimbal axis torque [2]. Thus SGCMG has become an ideal actuator for spacecraft attitude control and been widely investigated.

The output torque of an SGCMG is a processional, gyroscopic reaction torque perpendicular to both the rotor spin and gimbal axes due to torquing the gimbal [3]. Due to this geometric constraint, there will always exist some situations where all the output are collinear or coplanar. These situations are called singularity and the direction without output is called singular direction. Margulies and Aubrun established the mathematical foundation of singularity analysis [4]. Based on this work, Wie showed a novel viewpoint in characterizing and visualizing the physical as well as mathematical nature of the singularities in [3]. Then singularity problem for redundant or non-redundant system with respect to different SGCMG configurations has been addressed in [5], [6], [7].

Recently, Bhat, et al. has proved the controllability of the spacecraft containing one or more CMGs on the same momentum level. They also derived the sufficient condition for the controllability of a two-SGCMG spacecraft. It states that the spacecraft is controllable if the initial momentum of whole system is smaller than that of the CMGs [8]. This stimulates the interests in study of under-actuated spacecraft attitude control using two SGCMGs [9], [10], [11]. However, the significant obstacle of singularity still exists. Most of the existing works focus on the specific configuration they used: two parallel (coaxial) CMGs are employed and corresponding singularities are briefly introduced in [9], [12]; a pyramid-type two-CMG system and two-skew system (both belong to the non-coaxial configuration) with the singularity is studied in [11] and [12]. Extension from such a specific configuration to an arbitrary one is important so as to be applicable to the fault-tolerant control of a redundant system [13]. Then the under-actuated system will not only provide a fail-operation mode, but also improve the reliability of attitude control system, simplify collection of actuators, decrease cost and economize energy [14].

Motivated by the aforementioned observation, this paper builds a general frame to describe the two-CMG system. Since the gimbal axes are fixed in the spacecraft and the gimbal plane containing these two gimbals is unique for most of the cases, we can use this plane and the corresponding positive normal to build a unified frame and show a panorama of the two-CMG system regardless of the configuration. The cases when gimbals are parallel or anti-parallel can be easily transformed into an unified description. In this description, the angle between two fixed gimbal axes becomes a unique parameter to determine the shape of the momentum envelope and various singular surface, which offers the convenience for singularity analysis and configuration optimization. We show the singular surfaces with respect to different angles and propose some suggestions in choosing the optimal configuration.

2. UNIFIED COORDINATE FRAME

An SGCMG consisting of a spinning rotor fixed in a gimbal frame is shown in Fig. 1. The rotor spins along the axis $\hat{h}_i$

978-1-5090-1613-6/17/31.00 ©2017 IEEE

with a constant wheel speed Ω_i, the gimbal rotates along the gimbal axis $\hat{g}_i$ orthogonal to $\hat{h}_i$ with a gimbal angular velocity $\dot{\delta}_i$ and the gyroscopic output $\hat{\tau}_i = \hat{g}_i \times \hat{h}_i$ is perpendicular to both $\hat{g}_i$ and $\hat{h}_i$. These unit vectors form a CMG body coordinate denoted as $\mathbb{G}_i = \{\hat{g}_i, \hat{h}_i, \hat{\tau}_i\}$ with the subscript i denoting the ith CMG.

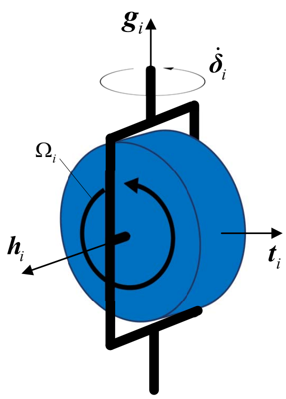

Figure 1. Schematic diagram of SGCMG

Firstly, we consider a two-CMG system with a non-coaxial configuration and the CMGs are denoted as CMG-i, CMG-$j(i \neq j; i,j = 1,2)$ as shown in Fig. 2. Since the gimbal axes are fixed, we can always define new vectors as:

$$\hat{h}_i = \hat{g}_i \times \hat{g}_j \ \left(\hat{h}_j = \hat{g}_j \times \hat{g}_i = -\hat{h}_i\right) \tag{1}$$

Also, we can define these vectors in an opposite way; i.e. $\hat{h}_i = \hat{g}_j \times \hat{g}_i$. What we need to do is to make the definition and the calculation be consistent. Then the new output torque direction can be obtained as:

$$\hat{\tau}_i = \hat{g}_i \times \hat{h}_j \ \left(\hat{\tau}_j = \hat{g}_j \times \hat{h}_j = \hat{h}_i \times \hat{g}_j\right) \tag{2}$$

After this definition, we obtain the unified CMG coordinate frame $\mathbb{G}_i = \{\hat{g}_i, \hat{h}_i, \hat{\tau}_i\}$ and $\mathbb{G}_j = \{\hat{g}_j, \hat{h}_j, \hat{\tau}_j\}$.

Now let us find the relationship of the new gimbal angle δ_i and the initial angle δ_{i0}. Notice that $\hat{h}_i^{'}$ traces the black circle which is orthogonal to gimbal axis $\hat{g}_i$ in the $\hat{h}_{i0} - \hat{\tau}_{i0}$ plane. As shown in Fig. 2, we can always find the intersection of the $\hat{h}_{i0} - \hat{\tau}_{i0}$ plane (marked as a black circle) and $\hat{g}_i - \hat{g}_j$ plane (marked as a red circle), which are $\hat{h}_i^{'}$ and $\hat{\tau}_i$. As an element in the $\hat{h}_{i0} - \hat{\tau}_{i0}$ plane, $\hat{h}_i^{'}$ can be expressed in the initial frame $\mathbb{G}_{i0}$:

$$\hat{h}_i^{'} = \cos\varphi_i \hat{h}_{i0} + \sin\varphi_i \hat{\tau}_{i0} \tag{3}$$

where φ_i is a negative gimbal angle. According to the figure, we can obtain $\hat{h}_i$ by rotating $\hat{h}_i^{'}$ 90 degree positively. Then we have

$$\begin{aligned} \hat{h}_i &= \cos\left(\varphi_i + \frac{\pi}{2}\right)\hat{h}_{i0} + \sin\left(\varphi_i \frac{\pi}{2}\right)\hat{\tau}_{i0} \\ &= -\sin\varphi_i \hat{h}_{i0} + \cos\varphi_i \hat{\tau}_{i0} \end{aligned} \tag{4}$$

Also we can replace $\varphi_i + \frac{\pi}{2}$ by $-\varphi_i - \frac{\pi}{2}$, which is determined by the definition (1).

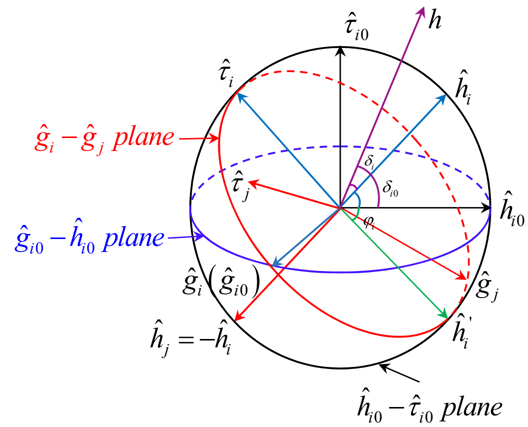

Figure 2. Principle in building unified frame

Since $\hat{h}_1$ is perpendicular to both of gimbal axes $\hat{g}_1$ and $\hat{g}_2$, we have:

$$\begin{cases} \hat{h}_1^T \hat{g}_1 = -\sin\varphi_1 \hat{h}_{10}^T \hat{g}_1 + \cos\varphi_1 \left(\hat{g}_1 \times \hat{h}_{10}\right)^T \hat{g}_1 = 0 \\ \hat{h}_1^T \hat{g}_2 = -\sin\varphi_1 \hat{h}_{10}^T \hat{g}_2 + \cos\varphi_1 \left(\hat{g}_1 \times \hat{h}_{10}\right)^T \hat{g}_2 = 0 \end{cases} \tag{5}$$

Similarly, we can find the relationship of $\hat{h}_2$ with $\hat{g}_1$ and $\hat{g}_2$:

$$\begin{cases} \hat{h}_2^T \hat{g}_1 = -\sin\varphi_2 \hat{h}_{20}^T \hat{g}_1 + \cos\varphi_2 \left(\hat{g}_2 \times \hat{h}_{20}\right)^T \hat{g}_1 = 0 \\ \hat{h}_2^T \hat{g}_2 = -\sin\varphi_2 \hat{h}_{20}^T \hat{g}_2 + \cos\varphi_2 \left(\hat{g}_2 \times \hat{h}_{20}\right)^T \hat{g}_2 = 0 \end{cases} \tag{6}$$

Solving equation (5) and (6), we obtain the angles φ_1 and φ_2. Then the gimbal angle expressed in the unified frame can be re-expressed as:

$$\delta_i = \delta_{i0} - \left(\varphi_i + \frac{\pi}{2}\right) = \delta_{i0} - \varphi_i - \frac{\pi}{2}(i = 1,2) \tag{7}$$

Secondly, we assume that the gimbal axes are collinear; i.e. $\hat{g}_1 = \hat{g}_2$ or $\hat{g}_1 = -\hat{g}_2$. In such an occasion, the gimbal plane is not unique. We need to modify the definition to guarantee the feasibility of the unified frame for this case. To simply the transformation, we can make one of new frames be consistent with the original one. Without loss of generality, we choose $\hat{g}_1 = \hat{g}_2$ and $\hat{\tau}_1 = \hat{\tau}_{10}$. Then $\hat{h}_2 = -\hat{h}_{10}$ and $\hat{\tau}_2 = \hat{h}_{10} \times \hat{g}_2$. Also we can obtain the current gimbal angle as $\delta_1 = \delta_{10}$, $\delta_2 = \delta_{20} + \varphi$ with φ determined by the relative position of $\hat{h}_2$ and $\hat{h}_2$.

Hence, for any configuration of the two-SGCMG system, the angular moment and output torque can be expressed as:

$$\begin{cases} h_i = h_0 \cos\delta_i \hat{h}_i + h_0 \sin\delta_i \hat{\tau}_i \\ \quad = h_0 \cos\delta_i \left[\hat{g}_i \times \hat{g}_j\right] + h_0 \sin\delta_i \left[\hat{g}_i \times (\hat{g}_i \times \hat{g}_j)\right] \\ \tau_i = -\dot{\delta}_i h_0 \sin\delta_i \hat{h}_i + \dot{\delta}_i h_0 \cos\delta_i \hat{\tau}_i \\ \quad = -\dot{\delta}_i h_0 \sin\delta_i \left[\hat{g}_i \times \hat{g}_j\right] + \dot{\delta}_i h_0 \cos\delta_i \left[\hat{g}_i \times (\hat{g}_i \times \hat{g}_j)\right] \end{cases} \tag{8}$$

with h_0 and $\dot{\delta}_i$ being the angular momentum of the rotor and gimbal angular velocity.

Example 2.1 Traditional pyramids configuration

For the typical pyramid configuration, the gimbal axes matrix $G = [g_1 \quad g_2 \quad g_3 \quad g_4]$ and $H = \begin{bmatrix}\hat{h}_{10} & \hat{h}_{20} & \hat{h}_{30} & \hat{h}_{40}\end{bmatrix}$ are:

$$G = \begin{bmatrix} s\beta & 0 & -s\beta & 0 \\ 0 & -s\beta & 0 & s\beta \\ c\beta & c\beta & c\beta & c\beta \end{bmatrix}, H = \begin{bmatrix} 0 & -1 & 0 & -1 \\ 1 & 0 & -1 & 0 \\ 0 & 0 & 0 & 0 \end{bmatrix}$$

with $s\beta$ representing $\sin\beta$, $c\beta$ representing $\cos\beta$ and β being the skew angle.

In this example, we will show how to describe the system in the unified frame for CMG $(1,2)$ pair and CMG $(1,3)$ pair.

a). CMG $(1,2)$ pair

According to definition (1), we have

$$\begin{cases} \hat{h}_1 = \hat{g}_1 \times \hat{g}_2 = p[c\beta \quad -c\beta \quad -s\beta]^T \\ \hat{h}_2 = \hat{g}_2 \times \hat{g}_1 = p[-c\beta \quad c\beta \quad s\beta]^T = -\hat{h}_1 \end{cases}$$

$$\begin{cases} \hat{\tau}_1 = \hat{g}_1 \times \hat{h}_1 = p\begin{bmatrix}\mathrm{c}^2\beta & 1 & -\mathrm{s}\,\beta\,\mathrm{c}\,\beta\end{bmatrix}^T \\ \hat{\tau}_2 = \hat{g}_2 \times \hat{h}_2 = p\begin{bmatrix}-1 & -\mathrm{c}^2\beta & -\mathrm{s}\,\beta\,\mathrm{c}\,\beta\end{bmatrix}^T \end{cases}$$

where $p = 1/\sqrt{1+\mathrm{c}^2\beta}$. According to relationship (3) to (5), we have

$$\varphi_i = \arccos\left(\hat{h}_i^T \hat{h}_{i0}\right) - \frac{\pi}{2} \tag{9}$$

Thus

$$\begin{cases} \varphi_1 = \arccos\left(-pc\beta\right) - \dfrac{\pi}{2} \\ \varphi_2 = \arccos\left(pc\beta\right) - \dfrac{\pi}{2} \end{cases}$$

b). CMG $(1,3)$ pair

For CMG $(1,3)$ pair, we can easily obtain

$$\begin{cases} \hat{h}_1 = [0 \quad -1 \quad 0]^T = -\hat{h}_{10} \\ \hat{h}_3 = [0 \quad 1 \quad 0]^T = -\hat{h}_{30} \end{cases}$$

$$\begin{cases} \hat{\tau}_1 = [\cos\beta \quad 0 \quad -\sin\beta]^T = -\hat{\tau}_{10} \\ \hat{\tau}_3 = [-\cos\beta \quad 0 \quad -\sin\beta]^T = \hat{\tau}_{30} \end{cases}$$

and

$$\varphi_1 = \varphi_3 = \frac{\pi}{2}$$

Remark 1: In case b), the unified frame is obtained by rotating 180 degree along the gimbal axis. Obviously it's useless to make such a transformation. Actually, we can modify the definition of equation (1) by $\hat{h}_i = \hat{g}_j \times \hat{g}_i$. Then the unified frame will be consistent with the initial frame.

Example 2.2 Coaxial configuration

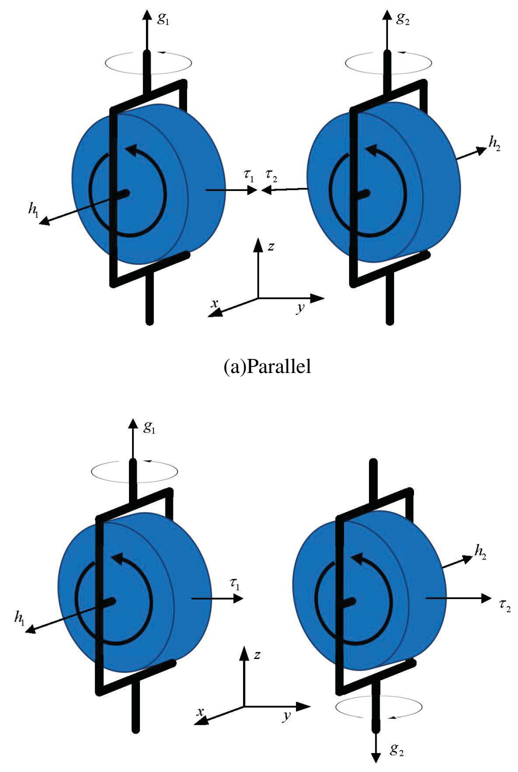

(a)Parallel

(b)Anti-parallel

Figure 3. Coaxial configuration

Both the parallel and anti-parallel configurations are demonstrated in Fig. 3. It is clear from Fig. 3(a) and Fig. 3(b) that the angular momentum of each rotor are in opposite directions. This observation is consistent with the definition of the unified coordinate frame. Thus Fig. 3 shows the typical unified frame for the coaxial configuration.

In other cases, it is easy to transform the initial frame $\mathbb{G}_{i0}$ into $\mathbb{G}_i$. First, we can find the corresponding $\hat{h}_j$ by choosing the opposite direction of $\hat{h}_i$. Then the angle difference between δ_i and δ_{i0} is easy to compute because $\hat{h}_i$ tracks a circle in a unique plane which is perpendicular to $\hat{g}_i$ and passes $\hat{h}_{i0}$.

3. Singularity Analysis

In the previous section, we introduce a unified frame to describe the two-SGCMG system. Such a frame is built on the basis of the gimbal plane and its positive normal. On the same basement, we can construct a body frame $\mathbb{B} = \{\mathbb{X}, \mathbb{Y}, \mathbb{Z}\}$ as shown in Fig. 4. First, we assume that the CMGs are in non-coaxial configuration, which is convenient to define the body frame and the coaxial configuration will be regarded as a particular case. Then Z axis is defined along the direction of $\hat{g}_1 \times \hat{g}_2$; i.e. the direction of $\hat{h}_1$; Y axis is along the intermediate direction of $\hat{g}_1$ and $\hat{g}_2$; i.e. the direction of $\hat{g}_1 + \hat{g}_2$; X axis forms a right-hand coordinate frame together with Y and Z. The skew angle between the two gimbals is denoted as θ, which belongs to the interval $[0, \pi]$.

According to the definition, the gimbal axes can be written

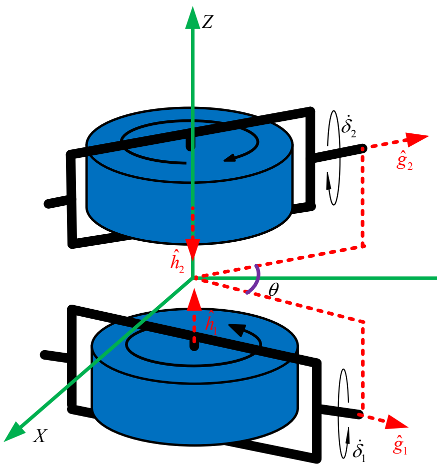

Figure 4. Configuration of the CMGs in body frame

as:

$$\hat{g}_1 = \begin{bmatrix} \mathrm{s}(\theta/2) \\ \mathrm{c}(\theta/2) \\ 0 \end{bmatrix}, \hat{g}_2 = \begin{bmatrix} -\mathrm{s}(\theta/2) \\ \mathrm{c}(\theta/2) \\ 0 \end{bmatrix} \tag{10}$$

and the angular momentum axes can be expressed as:

$$\hat{h}_1 = \begin{bmatrix} 0 \\ 0 \\ 1 \end{bmatrix}, \hat{h}_2 = \begin{bmatrix} 0 \\ 0 \\ -1 \end{bmatrix}, \hat{\tau}_1 = \begin{bmatrix} \mathrm{c}(\theta/2) \\ -\mathrm{s}(\theta/2) \\ 0 \end{bmatrix}, \hat{\tau}_2 = \begin{bmatrix} -\mathrm{c}(\theta/2) \\ -\mathrm{s}(\theta/2) \\ 0 \end{bmatrix} \tag{11}$$

Assuming the gimbal angles are δ_1 and δ_2 respectively, we obtain h_1 and h_2 from equation (3):

$$h_1 = h_0 \begin{bmatrix} \mathrm{s}\,\delta_1\,\mathrm{c}(\theta/2) \\ -\mathrm{s}\,\delta_1\,\mathrm{s}(\theta/2) \\ \mathrm{c}\,\delta_1 \end{bmatrix}, h_2 = h_0 \begin{bmatrix} -\mathrm{s}\,\delta_2\,\mathrm{c}(\theta/2) \\ -\mathrm{s}\,\delta_2\,\mathrm{s}(\theta/2) \\ -\mathrm{c}\,\delta_2 \end{bmatrix} \tag{12}$$

and the output torque:

$$\tau = \tau_1 + \tau_2 = h_0 \begin{bmatrix} c\delta_1\,\mathrm{c}(\theta/2) & -c\delta_2\,\mathrm{c}(\theta/2) \\ -c\delta_1\,\mathrm{s}(\theta/2) & -c\delta_2\,\mathrm{s}(\theta/2) \\ -s\delta_1 & s\delta_2 \end{bmatrix} \begin{bmatrix} \dot{\delta}_1 \\ \dot{\delta}_2 \end{bmatrix} = h_0 A \dot{\delta} \tag{13}$$

In the following simulation, h_0 will be assumed to be $1Nm$.

A. Angular momentum

Equation (12) demonstrates the angular momentum of each CMG, and then the total angular momentum is obtained as:

$$h = h_0 \begin{bmatrix} (\mathrm{s}\,\delta_1 - \mathrm{s}\,\delta_2)\,\mathrm{c}(\theta/2) \\ -(\mathrm{s}\,\delta_1 + \mathrm{s}\,\delta_2)\,\mathrm{s}(\theta/2) \\ \mathrm{c}\,\delta_1 - \mathrm{c}\,\delta_2 \end{bmatrix} \tag{14}$$

It is clear that $h_y = 0$ when $\theta = 0$, and then the angular momentum vector will stay in the $h_x - h_z$ plane as shown in Fig. 5(a). When θ varies from 0° to 90°, the attainable momentum grows from a planar disk to a uniformly distributed 3-dimensional sphere, with four inwards trumpets removed from the sphere along the $X/-X$ and $Y/-Y$ axes. All the spheres share a similar shape as shown in Fig. 5(b) and are distinguished by the attainable momentum magnitude along X and Y axes. When θ continues to grow from 90° to 180°, the sphere loses weight in the X axis orthogonal to Y in which direction it grows fatter, and finally degenerates to a planar disk as in Fig. 5(c).

Remark 2: *It can be concluded from the above analysis that θ determines the distribution of angular momentum in the 3-dimensional space and has the largest and most uniformly distributed volume when $\theta = 90°$.*

From equation (14), we can get the magnitude of the momentum as:

$$\begin{aligned} H &= \|h\|_2{}^2 = h_0{}^2\,(2 - 2\sin\delta_1\sin\delta_2\cos\theta - 2\cos\delta_1\cos\delta_2) \\ &= h_0{}^2\,(2 + (\cos\alpha - \cos\beta)\cos\theta - (\cos\alpha + \cos\beta)) \end{aligned} \tag{15}$$

with $\alpha = \delta_1 + \delta_2, \beta = \delta_1 - \delta_2$.

a) When $\theta = 0°$, Eq (15) becomes $H = h_0{}^2\,(2 - 2\cos\beta)$. The maximum occurs at $\beta = (2k+1)\,\pi, (k \in Z)$, namely $\delta_1 = \delta_2 + (2k+1)\,\pi, (k \in Z)$. The minimum locates at the straight line $\beta = 2k\pi, (k \in Z)$; i.e. $\delta_1 = \delta_2 + 2k\pi, (k \in Z)$. This is demonstrated in Fig. 6(a).

b) When $\theta = 180°$, it becomes $H = h_0{}^2\,(2 - 2\cos\alpha)$. Consequently, the maximum and minimum occur at $\alpha = (2k+1)\,\pi, (k \in Z)$, and $\alpha = 2k\pi, (k \in Z)$, which is $\delta_1 = -\delta_2 + (2k+1)\,\pi, (k \in Z)$ and $\delta_1 = -\delta_2 + 2k\pi, (k \in Z)$ respectively. This is demonstrated in Fig. 6(f).

c) When θ varies in the interval $(0, \pi/2)$, the peak and valley will be staying on the straight line determined by $\theta = 0°$. However, subsidence and uplift occurs at the peak and valley and they reach the same height when $\theta = 90°$. Afterwards, the subsidence goes down and uplift rises up to form a new valley and peak determined by $\theta = 180°$. This trend is shown in Fig. 6 with θ going from 0° to 180°.

Remark 3: *As seen in the aforementioned observation, θ influences the distribution of momentum magnitude. When $\theta = 90°$, the peaks and valleys are uniformly distributed.*

B. Singular surface

Noticing that $rank\,(A) \le 2$, thus the two-CMG is always singular and the singular direction τ_s can be directly computed as:

$$\tau_s = \tau_1 \times \tau_2 = \begin{bmatrix} -s\,(\delta_1 + \delta_2)\,s\,(\theta/2\,) \\ s\,(\delta_1 - \delta_2)\,c\,(\theta/2\,) \\ c\delta_1 c\delta_2 s\theta \end{bmatrix} \tag{16}$$

It is clear that $\tau_s = [0 \quad 1 \quad 0]^T$ and $\tau_s = [1 \quad 0 \quad 0]^T$ when $\theta = 0°$ and $\theta = 180°$ respectively, which means the output torque will be constrained in the $x - z$ plane and $y - z$ plane as well as the angular momentum. From another aspect, $\delta_1 = \delta_2 + k\pi$ results in $\tau_s(x) = 0$ no matter how θ varies. Similarly, $\delta_1 = -\delta_2 + k\pi$ results in $\tau_s(y) = 0$. These conditions are consistent with the peak and valley condition in analyzing the magnitude of the momentum. Thus the singularity can be reflected by the distribution of angular momentum, and one classical method is the cutting plane technique.

Since only two CMGs are installed, there will be two categories of singularity: 2H and 0H. In 2H singularity, all the angular momentum vectors are located in the same side of the plane, which is orthogonal to the singular direction and contains all the output torques. This type of singularity reflects the maximum angular projection onto the singular direction and leads to the saturation. If one of the angular momentum

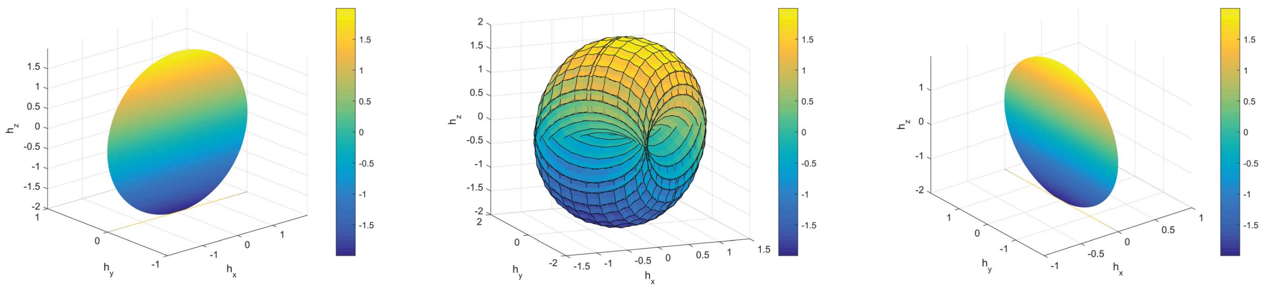

(a)$\theta = 0°$ (b)$\theta = 90°$ (c)$\theta = 180°$

Figure 5. Angular momentum

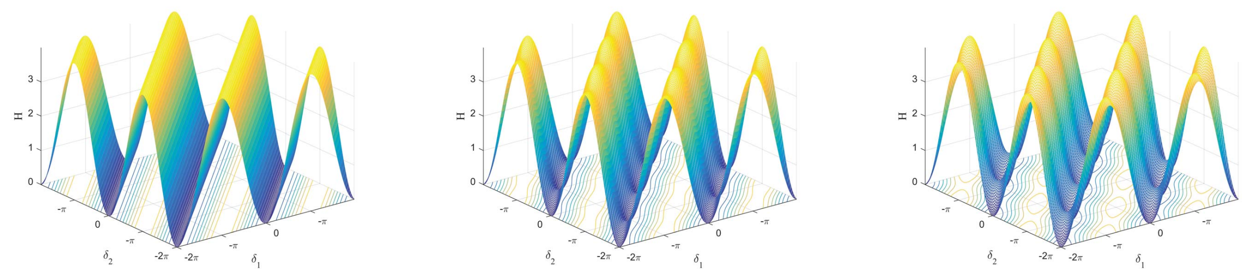

(a)$\theta = 0°$ (b)$\theta = 30°$ (c)$\theta = 45°$

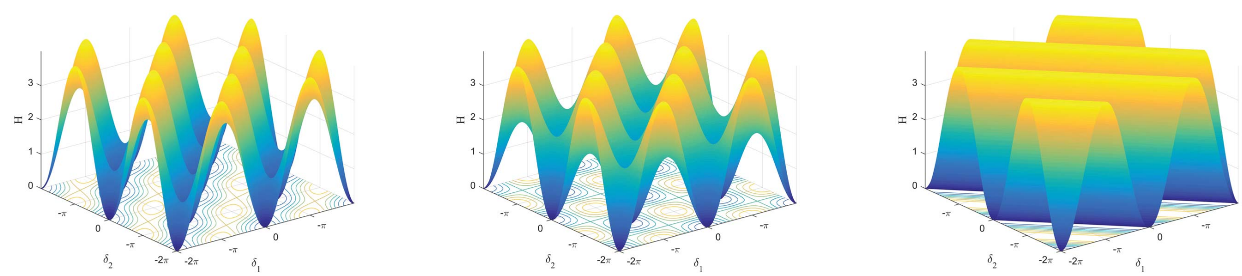

(d)$\theta = 60°$ (e)$\theta = 90°$ (f)$\theta = 180°$

Figure 6. Influence of θ on the momentum magnitude

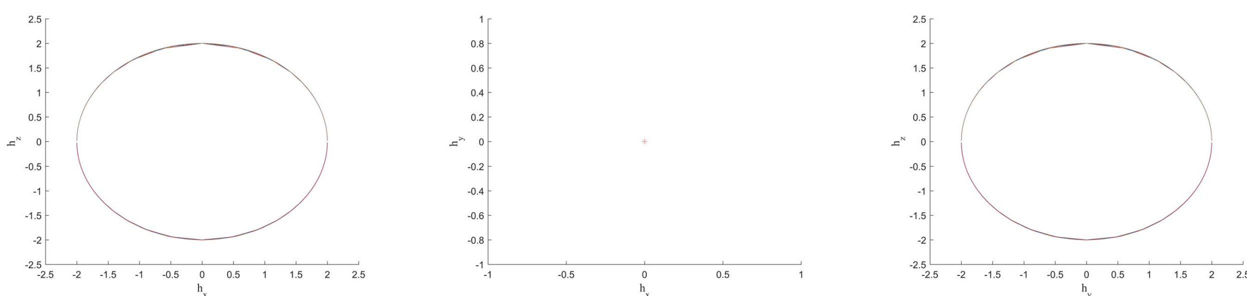

(a)2H surface with $\theta = 0°$ (b)0H surface with $\theta = 0°/180°$ (c)2H surface with $\theta = 180°$

Figure 7. Attainable singular surface with $\theta = 0°$ or $\theta = 180°$

vector is reversed, the 0H singularities are determined.

For visualization and simulation, we can parameterize the singular direction on the S^2 surface with a spherical coordinate as:

$$u = \begin{bmatrix} \cos(\varphi)\cos(\lambda) & \cos(\varphi)\sin(\lambda) & \sin(\lambda) \end{bmatrix}^T$$

with $\lambda \in [-\pi, \pi], \varphi = \left[-\frac{\pi}{2}, \frac{\pi}{2}\right]$. When the singularity occurs, the output torque lies in the plane orthogonal to the singular direction. Then we can get the ith output as:

$$\tau_i = \epsilon_i \frac{g_i \times u}{|g_i \times u|} = \epsilon_i \frac{g_i \times u}{\sqrt{1 - (g_i \cdot u)^2}}$$

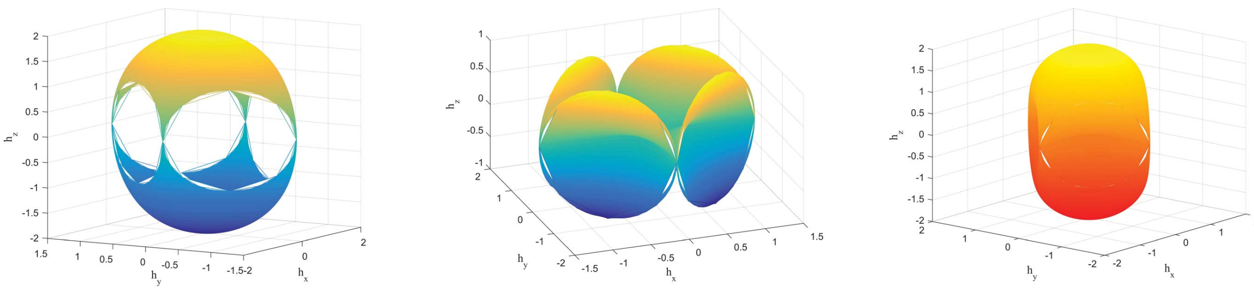

(a)2H surface with $\theta = 90°$ (b)0H surface with $\theta = 90°$ (c)Singular surface with $\theta = 90°$

Figure 8. Attainable singular surface with $\theta = 90°$

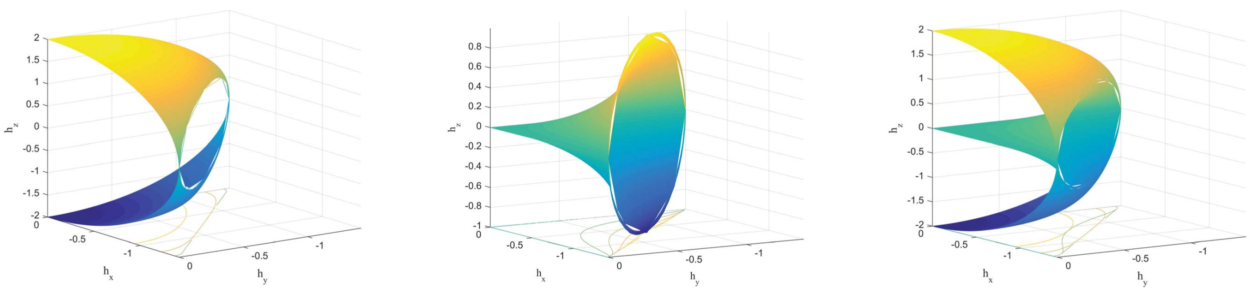

(a)Quarter of 2H surface with $\theta = 0°$ (b)Quarter of 0H surface with $\theta = 0°/180°$ (c)Quarter of singular surface with $\theta = 180°$

Figure 9. Decomposition of singular surface with $\theta = 0°$ or $\theta = 180°$

with $\epsilon_i = \pm 1$ being direction of the output torque. By the definition of the $\mathbb{G}_i$, ith angular momentum can be expressed as:

$$h_i = \tau_i \times g_i = \epsilon_i \frac{(g_i \times u) \times g_i}{|g_i \times u|} = \epsilon_i \frac{u - (g_i \cdot u) g_i}{|g_i \times u|}$$

When all the ϵ_i are positive or negative, 2H surface is obtained as shown in 8(a) and 9(a). When one of the ϵ_i is reversed, $0H$ surface is obtained as in 8(b) and 9(b).

Illustrated as 8(a), 2H singular surface (saturation singular surface) is a sphere with four disks removed along the $X/-X$ and $Y/-Y$ axes. A detailed quarter of this surface is shown in 9(a). From the projection of the surface on the $h_x - h_y$ plane, it seems that the sphere is cut by a plane and a circular hole is remained. On the contrary to the 2H surface, that is a part of the external boundary of the momentum envelope, 0H surface is the internal singularity. It is composed of four trumpets and intersected at the origin as demonstrated in 8(b) and 9(b). These two manifolds of 2H and 0H surfaces are connected at the four sharp points in $X - Y$ plane; i.e. $\delta_1 = \delta_2 = \pi/2$, $\delta_1 = \delta_2 = 3\pi/2$, $\delta_1 = \pi/2, \delta_2 = 3\pi/2$ or $\delta_1 = 3\pi/2, \delta_2 = \pi/2$. These points correspond to those who make $\tau_s = 0$.

4. Configuration Optimization

For the CMG-actuated attitude control system, the controllability and the complexity of the steering law are the two main concerns. According to [8], spacecraft is controllable only when the CMG angular momentum is larger than that of the overall system. Thus enlarging the angular momentum will increase the feasiblity and diversity of the control mission. However, with the increasement of the moment envelope, the complexity of the singularity increases, which in turn adds the complexity of the steering law. Thus it limits the application in real mission.

A. Optimization about momentum

Bhat gives the controllability condition of CMG system [8]. Bayadi, et al. [15] and Gui, et al. [14] analyzed the local controllability of two-SGCMG system and pointed out that the spacecraft-CMG system is locally controllable when the total angular momentum is zero. This implies that angular momentum of the overall system should be completely under the control capacity of the CMG array.

Instead of regarding the CMG as a pure actuator, we consider the combined dynamic of the spacecraft-CMG system. Then the angular momentum of CMG array is the control signal, which is

$$u = \begin{bmatrix} u_1 \\ u_2 \\ u_3 \end{bmatrix} = h_0 \begin{bmatrix} (s\delta_1 - s\delta_2)\, c\,(\theta/2\,) \\ -(s\delta_1 + s\delta_2)\, s\,(\theta/2\,) \\ c\delta_1 - c\delta_2 \end{bmatrix} \tag{17}$$

We can easily verify that $h_1 \in [-2h_0 c\,(\theta/2\,), 2h_0 c\,(\theta/2\,)]$, $h_2 \in [-2h_0 s\,(\theta/2\,), 2h_0 s\,(\theta/2\,)]$ and $h_2 \in [-2h_0, 2h_0]$. Then the angular momentum will contain a sphere of radius $r = \min\{h_0 c\,(\theta/2\,), h_0 s\,(\theta/2\,)\}$ with $\theta \in \left(0^{\circ}, 180^{\circ}\right)$.

Then the optimization objective is to find the optimal θ to maximize the radius r, i.e:

$$\theta_{opt} = \max r\,(\theta) = \max\{\min\{h_0 c\,(\theta/2\,), h_0 s\,(\theta/2\,)\}\} \tag{18}$$

The optimal solution occurs when $\theta = 90°$ and the maximum $r = sqrt(2)/2h_0$. The optimized angular momentum is shown in Fig. 5(b).

B. Optimization about steering law

When the CMGs are viewed as pure actuators, steering logic is necessary to map the control command into the gimbal angular rate. The steering algorithm is to find a solution of gimbal states that accurately map the desired output torque to the SGCMG array while minimizing torque error and/or the amount of gimbal actuation used [16]. Existing steering laws can be categorized into singular avoidance, singular escape and hybrid logics [17], [18]. When the singularities are elliptic or impassable, singular avoid strategies are invalid. Then singular escape algorithms are essential, which, however, leads to a torque error.

Due to the induced torque error, the simpler the singular surface, the higher the ideal attitude control precision. Then it seems that the co-axial configuration poses an advantage. However, the initial condition with both δ_1 and δ_2 equal to zero is an elliptic singular case. This implies the high precision attitude control is destroyed at the beginning of maneuver. It's quite undesirable. Besides, the small time locally controllability is not guaranteed since there's no 3-dimensional sphere to contain the origin as its interior point. Combined with the optimization result determined from the viewpoint of controllability, $\theta = 90°$ is the optimal choice of the skew angle between the two gimbal axes.

5. Conclusion

A unified coordinate frame based on the unique feature of the CMG configuration has been introduced. Based on the unified frame, the angular momentum and the output torque are restated. Then the singular characteristics are presented and visualized. The CMG configuration has been optimized from the viewpoint of controllability and steering law. The optimized skew angle is concluded to be $\pi/2$. This work can be a guide to the under-actuated control system using two SGCMGs.

References

[1] Bong Wie, David Bailey, and Christopher Heiberg. Singularity robust steering logic for redundant single-gimbal control moment gyros. *Journal of Guidance, Control, and Dynamics*, 24(5):865–872, 2001.

[2] Kevin A. Ford and Christopher D. Hall. Singular direction avoidance steering for control-moment gyros. *Journal of Guidance, Control, and Dynamics*, 23(4):648–656, 2000.

[3] Bong Wie. Singularity analysis and visualization for single-gimbal control moment gyro systems. *Journal of Guidance, Control, and Dynamics*, 27(2):271–282, 2004.

[4] Margulies G. and Aubrun. Geometric theory of single-gimbal control moment gyro systems. *Journal of the Astronautical Sciences*, 26(2):159–191, 1978.

[5] Alice Giffen. *Singular Structure of CMG Systems*. University of Surrey, GU2 7XH, UK, 2010.

[6] Frederick A. Leve, Brian J. Hamilton, and Mason A. Peck. *Spacecraft Momentum Control Systems*, volume 1010.

[7] Timothy Sands, Jae Jun Kim, and Brij N. Agrawal. Nonredundant single-gimbaled control moment gyroscopes. *Journal of Guidance, Control, and Dynamics*, 35(2):578–587, 2012.

[8] Sanjay P. Bhat and Pawan K. Tiwari. Controllability of spacecraft attitude using control moment gyroscopes. *IEEE Transactions on Automatic Control*, 54(3):585–590, 2009.

[9] Lei Jin and Shijie Xu. Underactuated spacecraft angular velocity stabilization and three-axis attitude stabilization using two single gimbal control moment gyros. *Acta Mechanica Sinica*, 26(2):279–288, 2010.

[10] Sangwon Kwon, Takashi Shimomura, and Hiroshi Okubo. Pointing control of spacecraft using two SGCMGs via LPV control theory. *Acta Astronautica*, 68(7):1168–1175, 2011.

[11] Shinya Kasai, Hirohisa Kojima, and Mitsunori Satoh. Spacecraft attitude maneuver using two single-gimbal control moment gyros. *Acta Astronautica*, 84:88–98, 2013.

[12] Haichao Gui, Lei Jin, Shijie Xu, and Jun Zhang. On the attitude stabilization of a rigid spacecraft using two skew control moment gyros. *Nonlinear Dynamics*, 79(3):2079–2097, 2015.

[13] Katsuhiko Yamada, Ichiro Jikuya, and Okgyu Kwak. Rate damping of a spacecraft using two single-gimbal control moment gyros. *Journal of Guidance, Control, and Dynamics*, 36(6):1606–1623, 2013.

[14] Haichao Gui, Lei Jin, and Shijie Xu. Local controllability and stabilization of spacecraft attitude by two single-gimbal control moment gyros. *Chinese Journal of Aeronautics*, 26(5):1218–1226, 2013.

[15] Ramaprakash Bayadi, Ravi N. Banavar, and Bernhard M. Maschke. Small-time local controllability of the orientation of a spacecraft actuated by cmgs. In *Proc. of the 18 IFAC World Congress, Milano, Italy, September*, pages 13828–13833, 2011.

[16] Junkins J. L. and Kim Y. Introduction to dynamics and control of flexible structures. *AIAA Education Series*, page 964, 1993.

[17] Frederick A. Leve and Norman G. Fitz-Coy. Hybrid steering logic for single-gimbal control moment gyroscopes. *Journal of Guidance, Control, and Dynamics*, 33(4):1202–1212, 2010.

[18] Haruhisa Kurokawa. Survey of theory and steering laws of single-gimbal control moment gyros. *Journal of Guidance, Control, and Dynamics*, 30(5):1331–1340, 2007.

Biography

***Cheng Fei Yue** received a B.Eng. degree in Flight Vehicle Design and Engineering from Honor School, Harbin Institute of Technology, Harbin, P.R.C in 2013. He is currently pursuing a Ph.D degree with the Department of Electrical and Computer Engineering, National University of Singapore, Singapore under the supervision of Prof Tong Heng Lee and Prof Cher Hiang Goh.*

His current research interests include under-actuated attitude control of spacecraft, modeling and simulation using control moment gyros and adaptive control.

Cher Hiang Goh *received a Dipl.-Ing. (equivalent M.Sc.) from Universiteat Paderborn, Germany in 1984 and a Dr.-Ing. (equivalent to Ph.D) in 1993 from Ruhr-Boechum Universitaet, Germany. His specialization is Mechanical Design, Automatic Control and Control of Space Flexible Structure. He is currently a Distinguished Member of the Technical Staff of DSO National Laboratories.*

He has been instrumental in building up micro-satellite capabilities in Singapore. From 2005-2011, he was seconded to NTU to be Project Director leading a team of 48 engineers to successfully design, develop, launch and operate the X-Sat satellite since its launch on 20 April 2011. From 2013 till now, he has been seconded to NUS and led the build-up of satellite capabilities in NUS. Here, he led a team to work with a collaborator on a micro-satellite project (Kent Ridge-1) and he is also an Advisor to a Nano-satellite project (Galassia). From 2012-2013, he was a Distinguished Visiting Professor to Naval Postgraduate School, USA.

He chaired the 1st Singapore Space Symposium in 2014 and was the General Co-chair of IEEE Asia Pacific Synthetic Aperture Radar Conference 2015. He is a Committee Member of IEEE AES-GRSS (Singapore Chapter). He is a Member of the Institute of Navigation; Senior Member of IEEE and AIAA.

Tong Heng Lee *received a B.A. degree with First Class Honours in the Engineering Tripos from Cambridge University, England, in 1980; the M.Engrg. degree from NUS in 1985; and the Ph.D degree from Yale University in 1987. He is a Professor in the Department of Electrical and Computer Engineering at the National University of Singapore (NUS); and also a Professor in the NUS Graduate School, NUS NGS. He was a Past Vice-President (Research) of NUS.*

Dr. Lee's research interests are in the areas of adaptive systems, knowledge-based control, intelligent mechatronics and computational intelligence. He currently holds Associate Editor appointments in the IEEE Transactions in Systems, Man and Cybernetics; Control Engineering Practice (an IFAC journal); and the International Journal of Systems Science (Taylor and Francis, London). In addition, he is the Deputy Editor-in-Chief of the IFAC Mechatronics journal.

Dr. Lee was a recipient of the Cambridge University Charles Baker Prize in Engineering; the 2004 ASCC (Melbourne) Best Industrial Control Application Paper Prize; the 2009 IEEE ICMA Best Paper in Automation Prize; and the 2009 ASCC Best Application Paper Prize. He has also co-authored five research monographs (books), and holds four patents (two of which are in the technology area of adaptive systems, and the other two are in the area of intelligent mechatronics). He is also a recipient of the 2013 ACA Wook Hyun Kwon Education Award in the area of Control Systems Engineering.

Qiang Shen *received a B.E. degree from Northwestern Polytechnical University, Xian, P.R. China, in 2010. He is currently working towards the Ph.D degree at Nanyang Technological University, Singapore. He is also an Associate Scientist in Temasek Laboratory of National University of Singapore since 2015. His research interests include fault-tolerant control and applications, spacecraft attitude control and control allocation.*